

Diffusive Liquid Propagation in Porous and Elastic Materials: The Case of Foams under Microgravity Conditions

A. Saint-Jalmes,¹ S. Marze,² H. Ritacco,² D. Langevin,² S. Bail,³ J. Dubail,³ L. Guingot,³ G. Roux,³
P. Sung,³ and L. Tosini³

¹*Groupe Matière Condensée et Matériaux, Université Rennes 1, Rennes, France*

²*Laboratoire de Physique des Solides, Université Paris-Sud, Orsay, France*

³*Ecole Polytechnique, Palaiseau, France*

(Received 13 April 2006; published 1 February 2007)

We report the results of fluid transport experiments in aqueous foams under microgravity. Using optical and electrical methods, the capillary motion of the foam fluid and the local liquid fractions are monitored. We show that foams can be continuously wetted up to high liquid fractions (~ 0.3), without any bubble motion instabilities. Data are compared to drainage models: For liquid fractions above 0.2, discrepancies are found and identified. These new results on foam hydrodynamics and structure can be useful for other poroelastic materials, such as plants and biological tissues.

DOI: [10.1103/PhysRevLett.98.058303](https://doi.org/10.1103/PhysRevLett.98.058303)

PACS numbers: 82.70.Rr, 68.03.-g

Aqueous foams, emulsions, as well as some gels, plants, and biological tissues are poroelastic materials: They are all fluid-infiltrated elastic cellular materials. In such soft and porous materials, the local liquid content and pore size are coupled to the elasticity of the matrix. Macroscopic motions (swelling or shrinking, for instance) are related to pressure gradients in the interstitial fluid, which consequently induce diffusive fluid transport [1,2]. In the case of aqueous foams, the bubbles are packed and deformed, and the liquid is confined in a network of interstitial channels [plateau borders (PBs)], interconnected by four at nodes, with the cross sections of these PBs and nodes depending on the liquid content ε [3,4]. The fluid in the PBs irreversibly flows (drainage), as a response to gravity and capillarity [5–7]. Foam drainage has been widely studied and is rather well understood; nevertheless, our understanding is not complete, especially as both experiments and models are limited to the range of low ε ($\varepsilon \leq 0.15$ for experiments, and $\varepsilon \leq 0.10$ for theory [5–8]). Indeed, when forcing liquid into a foam to make it wetter, convective instabilities occur [9,10], preventing access to high ε , which thus remain poorly understood. Besides the gravitational contribution, a capillary flow occurs in the case of a liquid fraction gradient: This implies a gradient in the fluid pressure P_L , tending to bring liquid from wet (high P_L) to dry parts of the foam (low P_L). Considering only these capillary effects, the situation in a foam thus resembles the one in plants and tissues: Liquid pressure gradients can induce an isotropic fluid flow, coupled to macroscopic strains via the elasticity of the solid matrix (for foams, the elastic modulus is set by γ/D , with γ the surface tension and D the bubble diameter [3,4]).

Studying capillary flows in foams can thus be an interesting approach to investigate the general features of fluid transport in soft and porous materials. Understanding the hydrodynamics across poroelastic materials is an impor-

tant issue to elucidate the origins and speed of observed natural movements [2], as well as for the development of hydraulically actuated soft systems and microfluidic devices. Using aqueous foams as a model system has some advantages: Experimental methods to measure local liquid fraction and models are already well developed. Microgravity conditions offer the opportunity to study solely capillary flows in foams. Attempts to decouple gravitational and capillary effects on the ground have been performed [11,12], but they remain always limited to low ε due to convective instabilities. In this Letter, we present fluid imbibition experiments in foams under microgravity. We show here that $\varepsilon \geq 0.3$ can be obtained when capillarity is the driving force. We then compare data to the classical drainage equations, in which gravity is set to zero, and discuss the validity of these equations throughout the liquid fraction range. In terms of the permeability of porous materials, we show that these new results allow us to fill the gap between systems of highly packed and deformed bubbles and systems of close-packed rigid spheres.

The experiments were performed during a parabolic flight campaign organized by the French space agency (CNES), providing 90 parabolas. For each parabola, 20 s of microgravity ($g \sim 0.1 \text{ m s}^{-2}$) are obtained, in between two equal periods of hypergravity ($g \sim 18 \text{ m s}^{-2}$). A normal gravity phase separates each parabola, lasting one or two minutes. Imbibition experiments are performed inside a transparent cell (height $H = 30 \text{ cm}$, width $W = 25 \text{ cm}$, thickness $T = 3 \text{ cm}$). The foam is made by bubbling air into a surfactant solution through a porous glass frit. This provides a mean bubble diameter $D = 3.2 \text{ mm}$, with a polydispersity lower than 20%. The surfactant aqueous solution is a mixture of sodium dodecyl sulfate (at 8 g/l) and dodecanol (at 0.3 g/l), providing a surface tension $\gamma = 32 \text{ mN/m}$ and a high bubble surface viscoelasticity. The experiment principle consists in injecting *continuously*

the same surfactant solution inside the foam, in the center of the cell, at flow rates Q varied from 4 to 80 ml/min. The injection starts at the beginning of the microgravity phase. Because of the previous hypergravity, the foam is always initially drained $\varepsilon_0 \sim 0.003$. As $sD < T \ll H, W$, this setup corresponds to a 2D propagation inside a 3D foam. To monitor the variations of ε in time and space, we have coupled electrical conductometry and light transmission measurements. A set of 24 electrodes is placed on each cell side, forming a cross centered on the injection point (Fig. 1). Thanks to a calibration between ε and the foam conductivity, the absolute liquid fraction is inferred [13]. The foam is also uniformly illuminated from one side, and a digital camera records the transmitted light: In the limit of multiple scattering, the wetter the foam, the darker it looks [14]. This technique is accurate for the detection of fluid front positions [7]. Note finally that previous imbibition studies in microgravity either dealt only with one layer of bubbles (2D foams) [15,16] or were still preliminary with 3D foams (focusing only on the front position) [17].

Many theoretical aspects of imbibition experiments in microgravity have been discussed in Ref. [18], starting from the drainage equations developed for ground experiments. These equations describe the time and space evolution of ε . A key point is that, depending on the bubble surface mobility M , different equations are found [18]. This surface mobility, initially introduced in Ref. [19], describes the coupling between flows inside the PBs and at their surfaces and is represented by a dimensionless number $M = \mu r / \mu_s$, where μ is the bulk viscosity, μ_s is the surface shear viscosity, and r is the PB radius of curvature [19,20]. The latter, for $\varepsilon < 0.1$, can be written $r = L\sqrt{\varepsilon}/\delta$, introducing the PB length L ($\delta = 0.41$ and

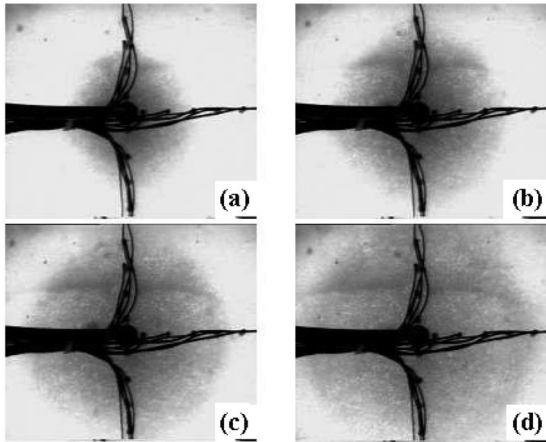


FIG. 1. Images in transmission at $t = 4, 7, 13,$ and 17 s after liquid injection at the center at $t = 0$ s. The white background is the initial dry foam ($\varepsilon_0 \sim 0.003$), and the foam is dark when wetted; at the front, the constant liquid fraction is ~ 0.005 , slightly above ε_0 . The dark cross corresponds to the conductivity electrodes and wires placed along two perpendicular directions. Image height = 12 cm and width = 15 cm.

$D = 2.7L$ for a Kelvin-type cell [4,5]). To model microgravity, the gravity term is removed in the equations, and one can write (the operators act on spatial coordinates) [18]:

$$\frac{\partial \varepsilon}{\partial t} = \nabla \cdot \left(\frac{\gamma \delta}{2\mu L} \varepsilon^s \nabla \varepsilon \right). \quad (1)$$

For low mobility M , $s = 0.5$ and the viscous dissipation takes place mainly within the PBs, while $s = 0$ corresponds to high mobility and high hydrodynamic resistances in the nodes [5,18]. In the case of liquid injection at a continuous Q , and for $s = 0.5$ (as expected for our solution [7]), one can find a solution for our experimental geometry (for the spatial coordinates, the cylindrical symmetry implies that only the radial distance R is needed):

$$\varepsilon = \bar{Q}^{2/3} f(\bar{R} \bar{t}^{-1/2} \bar{Q}^{-1/6}), \quad (2)$$

with $\bar{R} = R/L$, $\bar{t} = tK_r\gamma\delta/\mu L$, and $\bar{Q} = Q\mu/K_r\gamma\delta LT$. The dimensionless K_r is the foam permeability, which depends on M [7,20]. The function $f(x)$, describing the liquid fraction profile along a radius, verifies $x^2 f'(x) + 2[xf'(x)f(x)^{1/2}]' = 0$. There is no analytical solution for f ; numerically, it is found that f is a smoothly decreasing function (plotted in the inset in Fig. 3), with $f(x \geq 1.6) = 0$. Thus, at any time, there is a well-defined maximum distance R_f , covered by the fluid corresponding to $f = 0$ (R_f is called the front radius, though the shape of f does not strictly describe a front). In dimensional values, R_f is given by (for low M):

$$R_f = 0.8K_r^{1/3} Q^{1/6} t^{1/2}. \quad (3)$$

Also, it is found numerically that for a given t and R , $\varepsilon \sim Q^{4/5}$ and $\varepsilon \sim Q$ for low and high interfacial mobilities, respectively.

Figure 1 shows pictures in transmission of the foam at different times: in white is the initial dry foam, and in dark the wetted foam. The fluid propagation turns out to be isotropic: The contour of the wet part of the foam is always a circle, at any time and any flow rate Q . The front radius R_f is quantitatively determined by analyzing the intensity profile and by locating the frontier with the background level at ε_0 . R_f changes only with t and with Q , as shown in Fig. 2. For any Q , we find $R_f = At^{1/2}$, in agreement with Eq. (3), evidencing a diffusive transport. In the inset in Fig. 2, we have fitted with a power law the Q dependence of the prefactor A : An exponent 0.2 is found, close to the predicted value (1/6). The small discrepancy might be due to the low Q data for which the front radius is not big enough when compared to T , resulting in a not perfectly 2D situation.

We then extract from Fig. 2 the permeability K_r using Eq. (3): $K_r = 11.0 \pm 2 \times 10^{-3}$, in good agreement with other results and implying $M \approx 0.17$ [7,20]. We finally estimate a surface shear viscosity μ_s of about

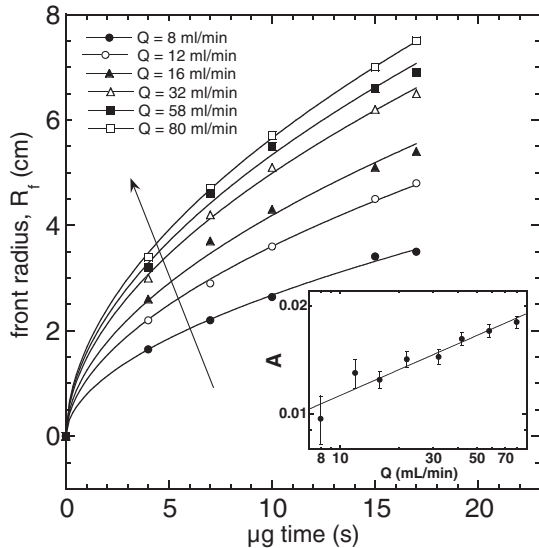


FIG. 2. Front position vs time, for different flow rates Q . Inset: Dependence of the prefactor A with Q . The lines are power law fits.

$10^{-6} \text{ kg s}^{-1}$, close to other estimates [7,21,22]. For this front propagation, and thus for $\varepsilon < 0.01$, data agree with the zero gravity equations, as also found in Ref. [17]. It is worth noting that, even if only capillarity is acting, the agreement between the models and data shows that the bulk-surface flow coupling is still valid and independent of the driving forces.

For any Q and at different t , the liquid fraction radial profiles can be constructed from the conductivity measurements, evidencing a smooth and curved shape, qualitatively similar to the predicted one (Fig. 3). The electrical measurements confirm that the propagation is isotropic, as no significant differences are found between perpendicular radii. Under these low gravity conditions, it is found that one can wet the foam continuously up to very high ε ($\varepsilon \sim 0.3$, at the electrode closest to the injection, for the highest Q). Thus, such experiments allow us to investigate for the first time hydrodynamics in foams of high ε . This wetting is obtained without any bubble motion or structure instabilities. Performing similar liquid injection experiments on the ground, at this bubble size, a critical fraction of 0.1 is found, above which the foam structure is destabilized [9]. The important difference between the ground and these experiments is the sharpness of the ε gradient, meaning that the rate at which ε changes is quite different. The time τ associated with the front and corresponding to the complete PB opening ($\tau > 10$ s here, and typically ≈ 1 s on the ground [5]) might be an important parameter controlling the onset of bubble position instability. If the flow rate is too high (above the instability threshold), implying too short a τ , the foam can no longer accommodate the gradient, and the structure gets destabilized in order to transport the fluid at the imposed flow rate. This qualitatively fits with the fact that the instability occurs at lower ε for

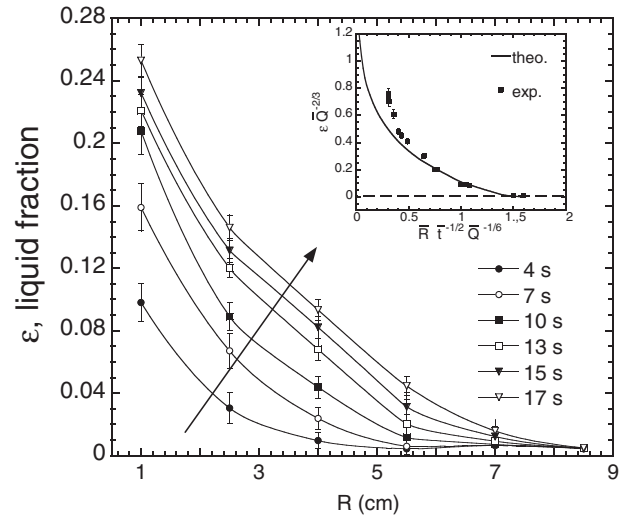


FIG. 3. For $Q = 58 \text{ ml/min}$, radial profiles of the liquid fraction at different times. The lines are guides for the eyes. The error bars represent the statistical data dispersion around average values (due to the bubble size or flow rate control). Inset: Theoretical profile for f , compared to data in dimensionless form [Eq. (2)].

bigger D (increasing D implies a sharper front) [9]. It is then tempting to make an analogy with instabilities seen in plants, where there is a minimal time for hydraulically swelling motion, above which instabilities also occur to allow faster motion [2].

Figure 4 shows the liquid fraction dependence with Q , at a radius $R = 1 \text{ cm}$ and at different times (the same trends are found at other R). It is possible to adjust the points with power law curves (dashed lines), and we find an exponent ≤ 1 for the short times (low ε) and closer to 0.75 for the longest times (high ε). As already stated, models provide $\varepsilon \sim Q^{4/5}$ or Q , depending on the mobility M . So, simply in terms of exponents, the measurements are consistent with the model. Note, though, that, despite different equations for $s = 0$ and $s = 0.5$, the predictions are quite similar and might be difficult to discriminate experimentally. Quantitatively, we can compute the liquid fraction evolution using Eq. (2), with the value K_r previously measured. We must recall that the model is valid only for dry foams, based on the assumption that the fluid is mainly within the PBs [4,5]. However, for $\varepsilon > 0.10$, the node volume is no longer negligible. Results of the simulations are also shown in Fig. 4: As expected, for $\varepsilon \leq 0.10$, we find a good quantitative agreement, but discrepancies occur as the liquid fraction increases. The discrepancy is also seen when trying to collapse the radial profiles of Fig. 3: All of the data points should collapse on the theoretical curve when plotting $\varepsilon \bar{Q}^{-2/3}$ vs $\bar{R} \bar{t}^{-1/2} \bar{Q}^{-1/6}$ [Eq. (2)]; a deviation, much bigger than the experimental precision (Fig. 3 inset), is found at the highest ε , as in Fig. 4. By analyzing for the first time the high ε and the behavior above the front (not done in Ref. [17]), we have thus found limits of the

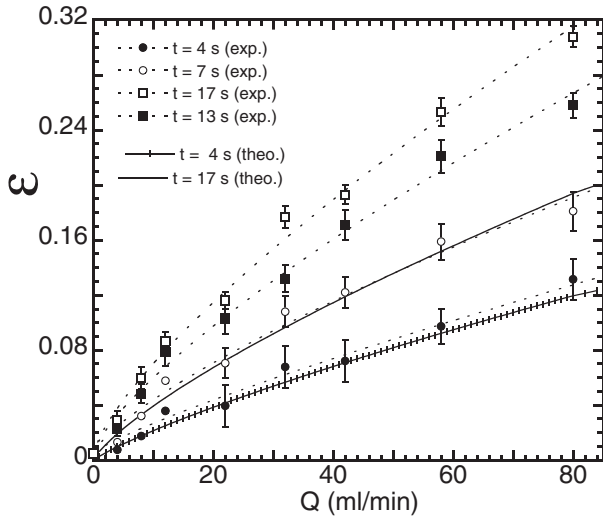


FIG. 4. Liquid fraction vs flow rate, at $R = 1$ cm, for different t . The dashed lines are power law fits. Simulations, for rigid interfaces and low node volume, for the two extreme times are shown.

drainage equations; the observed discrepancy means that the model overestimates the permeability. Forcing the agreement with the model implies that K_r decreases continuously down to $\sim 5 \times 10^{-3}$. This low value, below the theoretical limit of 6.6×10^{-3} for $M = 0$, and the fact that K_r decreases with ε (while it is expected to increase) also confirm that the model built for dry foams is not adapted and that not only the dissipation in the PBs must be taken into account for wet foams. However, it is instructive to compare the permeability value found here at the highest $\varepsilon > 0.25$ to the one of a close-packed bed of rigid spheres: For a fcc packing ($\varepsilon = 0.26$), Koehler *et al.* report that the permeability k can be written $k = 1.4 \times 10^{-3} L^2$ [5]. Expressed with K_r , one gets $K_r = k/(\varepsilon L^2)$, and then a value of $K_r = 5.4 \times 10^{-3}$ is predicted, actually close to our measured value. So, quantitatively, while at low ε the drainage equation well predicts the permeability, it becomes finally better described by a model of nondeformed packed spheres at the highest ε , showing that our data actually span over the whole range of possible packing.

In conclusion, we report here microgravity results of imbibition experiments in 3D foams, where the flow is due only to capillary pressure gradients. In the range of low liquid fractions, especially for the front propagation, we have found a good agreement between data and the drainage equation with $g = 0$. In that range, this theoretical framework developed for foams should be useful for any other soft and porous materials. However, as the liquid fraction increases, the limits of the model are well evidenced and are due to the failure of geometrical assump-

tions (neglecting the increased volume of the nodes). When the foam is wetted only by capillarity, it is a sufficiently smooth process, so that high liquid fractions can be reached, and no bubble structure instabilities are found. We have thus collected new and original data, increasing our understanding not only on foams but also on fluid transport in poroelastic materials and to which future models of such materials at high fluid contents could be compared.

The authors thank CNES and ESA (MAP program) for financial support.

-
- [1] M. Biot, *J. Appl. Phys.* **12**, 155 (1941).
 - [2] J.M. Skotheim and L. Mahadevan, *Science* **308**, 1308 (2005).
 - [3] R.K. Prud'homme and S.A. Khan, *Foams: Theory, Measurements, and Applications* (Marcel Dekker, New York, 1997).
 - [4] D. Weaire and S. Hutzler, *The Physics of Foams* (Oxford University, New York, 1999).
 - [5] S.A. Koehler, S. Hilgenfeldt, and H.A. Stone, *Langmuir* **16**, 6327 (2000).
 - [6] S.J. Cox, D. Weaire, S. Hutzler, J. Murphy, R. Phelan, and G. Verbist, *Proc. R. Soc. A* **456**, 2441 (2000).
 - [7] A. Saint-Jalmes, Y. Zhang, and D. Langevin, *Eur. Phys. J. E* **15**, 53 (2004).
 - [8] S.J. Neethling and H.T. Lee, and J. Cilliers, *J. Phys. Condens. Matter* **14**, 331 (2002).
 - [9] S. Hutzler, D. Weaire, and R. Crawford, *Europhys. Lett.* **41**, 461 (1998).
 - [10] M.U. Vera, A. Saint-Jalmes, and D.J. Durian, *Phys. Rev. Lett.* **84**, 3001 (2000).
 - [11] S.A. Koehler, S. Hilgenfeldt, and H.A. Stone, *Europhys. Lett.* **54**, 335 (2001).
 - [12] S. Hutzler, S. Cox, and G. Wang, *Colloids Surf. A* **263**, 178 (2005).
 - [13] K. Feitosa, S. Marze, A. Saint-Jalmes, and D.J. Durian, *J. Phys. Condens. Matter* **17**, 6301 (2005).
 - [14] M.U. Vera, A. Saint-Jalmes, and D.J. Durian, *Appl. Opt.* **40**, 4210 (2001).
 - [15] D. Noever and R.J. Cronise, *Phys. Fluids* **6**, 2493 (1994).
 - [16] H. Caps, S.J. Cox, H. Decauwer, D. Weaire, and N. Vandewalle, *Colloids Surf. A* **261**, 131 (2005).
 - [17] A. Saint-Jalmes, S. Marze, M. Safouane, and D. Langevin, *Microgravity Sci. Technol.* **18**, 5 (2006).
 - [18] S.J. Cox and G. Verbist, *Microgravity Sci. Technol.* **14**, 45 (2003).
 - [19] R.A. Leonard and R. Lemlich, *AIChE J.* **11**, 18 (1965).
 - [20] S.A. Koehler, S. Hilgenfeldt, and H.A. Stone, *J. Colloid Interface Sci.* **276**, 420 (2004).
 - [21] O. Pitois, C. Fritz, and M. Vignes-Adler, *Colloids Surf. A* **261**, 109 (2005).
 - [22] S.A. Koehler, S. Hilgenfeldt, and H.A. Stone, *J. Colloid Interface Sci.* **276**, 439 (2004).